Turbulent flow over a layer of a highly permeable medium simulated with a diffusion-jump model for the interface

Marcelo J.S. de Lemos *, Renato A. Silva

Departamento de Energia—IEME, Instituto Tecnológico de Aeronáutica—ITA, 12228-900 São José dos Campos, SP, Brazil

Abstract

Flow over a finite porous medium is investigated using different interfacial conditions. In such configuration, a macroscopic interface is identified between the two media. In the first model, no diffusion-flux is considered when treating the statistical energy balance at the interface. The second approach assumes that diffusion fluxes of turbulent kinetic energy on both sides of the interface are unequal. Comparing these two models, this paper presents numerical solutions for such hybrid medium, considering here a channel partially filled with a porous layer through which fluid flows in turbulent regime. One unique set of transport equations is applied to both regions. Effects of Reynolds number, porosity, permeability and jump coefficient on mean and turbulence fields are investigated. Results indicate that depending on the value of the stress jump parameter, substantially dissimilar fields for the turbulence energy are obtained. Negative values for the stress jump parameter give results closer to experimental data for the turbulent kinetic energy at the interface.
© 2005 Elsevier Ltd. All rights reserved.

Keywords: Turbulence modeling; Porous media; Volume-average; Time-average; Interface; Stress jump

1. Introduction

Investigation of flow over layers of permeable media has many applications in several environmental and engineering analyses. Turbulent atmospheric boundary layer over forests under fire [1], flow over vegetation and crop fields [2], currents at bottom of rivers [3], as well as grain storage and drying, can be characterized by some sort of porous layer over which a fluid permeates. Also, practical analysis of engineering flows can further benefit from more realistic mathematical and numerical modeling, as in the case of shell-and-tube heat exchangers [4] and nuclear reactor core [5], for example, where the rod bundles can be seen, in a macroscopic view, as a permeable medium.

When the domain of analysis presents a macroscopic interfacial area between a porous substrate and a clear flow region, the literature proposes the existence of a disconti-nuity in the momentum diffusion flux between the two media [6,7]. Analytical solutions involving such models have been published [8–10]. Also, in such works volume average properties for a homogenous treatment of flow in porous media are obtained by means of the volume-average theorem (VAT) [11,12].

Purely numerical solutions for two-dimensional hybrid medium (porous region-clear flow) in an isothermal channel have been considered in [13] based on the turbulence model proposed in [14–17]. That work has been developed under the double-decomposition concept [18–27]. Non-isothermal flows in channels past a porous obstacle [28] and through a porous insert have also been presented [29,30]. In all previous work of [13,28–30], the interface boundary condition considered a continuous function for the stress field across the interface.

Recently, the interface jump condition has been investigated for laminar flows, either considering non-linear effects in momentum equation as well as neglecting the Forchheimer term in the macroscopic model [31]. Therein, the authors simulated laminar flow over such interfaces

---

* Corresponding author. Tel.: +55 12 3947 5860; fax: +55 12 3947 5842.
E-mail address: delemos@mec.ita.br (M.J.S. de Lemos).

Nomenclature

c_F	Forchheimer coefficient in Eq. (4)
c_1, c_2	constants in Eq. (9)
c_k	constant in Eq. (8)
c_μ	constant in Eq. (7)
Da	Darcy number, $Da = K/H^2$
$\mathbf{D}$	deformation rate tensor, $\mathbf{D} = [\nabla\mathbf{u} + (\nabla\mathbf{u})^T]/2$
d	particle or pore diameter
G^i	production rate of k due to the porous matrix, $G^i = c_k \rho \phi \langle k \rangle^i |\bar{\mathbf{u}}_D|/\sqrt{K}$
H	distance between channel walls
$\mathbf{I}$	unit tensor
k	turbulent kinetic energy per unit mass, $k = \overline{\mathbf{u}' \cdot \mathbf{u}'}/2$
$\langle k \rangle^v$	volume (fluid + solid) average of k
$\langle k \rangle^i$	intrinsic (fluid) average of k
K	permeability
L	axial length of periodic section of channel
p	thermodynamic pressure
$\langle p \rangle^i$	intrinsic (fluid) average of pressure p
P^i	production rate of k due to mean gradients of $\bar{\mathbf{u}}_D$, $P^i = -\rho\langle\overline{\mathbf{u}'\mathbf{u}'}\rangle^i : \nabla\bar{\mathbf{u}}_D$
$\overline{\mathbf{R}}$	time average of total drag per unit volume
Re_H	Reynolds number based on the channel height, $Re_H = \frac{\rho|\bar{\mathbf{u}}_D|H}{\mu}$
s	clearance for unobstructed flow

S_φ	source term
$\bar{\mathbf{u}}$	microscopic time-averaged velocity vector
$\langle\bar{\mathbf{u}}\rangle^i$	intrinsic (fluid) average of $\bar{\mathbf{u}}$
$\bar{\mathbf{u}}_D$	Darcy velocity vector, $\bar{\mathbf{u}}_D = \phi\langle\bar{\mathbf{u}}\rangle^i$
$\bar{\mathbf{u}}_{D_i}$	Darcy velocity vector at the interface
$\bar{\mathbf{u}}_{D_p}$	Darcy velocity vector parallel to the interface
u_{D_n}, u_{D_p}	components of Darcy velocity at interface along η (normal) and ξ (parallel) directions, respectively
u_{D_i}, v_{D_i}	components of Darcy velocity at interface along x and y, respectively
x, y	Cartesian coordinates

Greek symbols

β	interface stress jump coefficient
μ	fluid dynamic viscosity
μ_{eff}	effective viscosity for a porous medium
μ_{t_ϕ}	macroscopic turbulent viscosity
ε	dissipation rate of k, $\varepsilon = \mu\overline{\nabla\mathbf{u}' : (\nabla\mathbf{u}')^T}/\rho$
$\langle\varepsilon\rangle^i$	intrinsic (fluid) average of ε
ρ	density
ϕ	porosity
$\boldsymbol{\varphi}$	general dependent variable
η, ξ	generalized coordinates

and validated their results against analytical solutions by [8–10]. Such work was based on the numerical methodology proposed for hybrid media and applied by [13,28–30]. The same numerical technique has been applied for computing turbulent flow [32] in a channel partially filled with a flat layer of porous material. Flows over wavy interfaces were also computed for both laminar [33] and turbulent flows [34]. There, the authors made use of the shear stress jump condition at the interface. Those works were also based on a numerical methodology specifically proposed for hybrid media [13,28–30].

A distinct line of investigation on turbulent flow over permeable media is based on the assumption that within the porous layer the flow remains laminar [35–38], which, in turn, precludes application of such methodology to flows through highly permeable media as atmospheric boundary layer over forests or crop fields.

Further, fine flow computations and experiments of flow over and inside a bed of rods in a two-dimensional channel have been presented [39]. Three-dimensional computational studies simulating flow over a layer formed by cubic blocks [40,41] also emphasize that depending on the permeable structure shape, turbulence may exists inside the porous bed and, as such, a turbulence model must be employed.

As seen, all models above considered either a flat or a rough (wavy) macroscopic interface limiting the porous

substrate. The stress jump condition for the momentum equations was applied, but in most publications so far, no such flux discontinuity for the $\langle k \rangle^v$-equation has been considered. Motivated by that, Refs. [42,43] proposed a model that assumes diffusion fluxes of turbulent kinetic energy on both sides of the interface to be unequal, which differs from all studies presented up to now. The purpose of this contribution is to explore and further document such proposal, investigating now its behavior as medium properties, such as permeability and porosity, are varied.

2. Macroscopic mathematical model

2.1. Geometry and governing equations

The flow under consideration is schematically shown in Fig. 1 where a channel is partially filled with a layer of a porous material. A constant property fluid flows longitudinally from left to right permeating through both the clear region and the porous structure. The case in Fig. 1 uses symmetry boundary condition at the channel center ($y = 0$). Also, $H = 10$ cm is the distance in between the channel walls and s the clearance for the non-obstructed flow passage. It should be emphasized that the class of flow under consideration involves porous substrates having a high porosity and permeability.
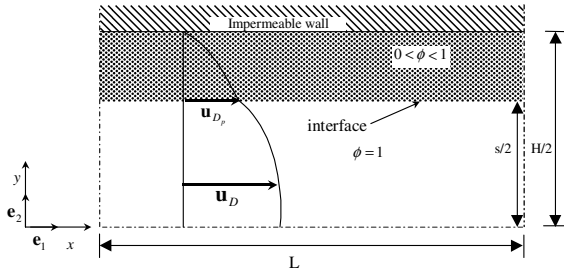
Fig. 1. Model for turbulent channel flow with porous material.

A macroscopic form of the governing equations is obtained by taking the volumetric average of the entire equation set. In this development, the porous medium is considered to be rigid and saturated by the incompressible fluid.

The macroscopic continuity equation is given by,

$$\nabla \cdot \bar{\mathbf{u}}_D = 0 \tag{1}$$

where the Dupuit–Forchheimer relationship, $\bar{\mathbf{u}}_D = \phi \langle \bar{\mathbf{u}} \rangle^i$, has been used and $\langle \bar{\mathbf{u}} \rangle^i$ identifies the intrinsic (liquid) average of the local velocity vector $\bar{\mathbf{u}}$ [12]. Eq. (1) represents the macroscopic continuity equation for an incompressible fluid in a rigid porous medium.

The macroscopic time-mean Navier–Stokes (NS) equation for an incompressible fluid with constant properties can be written as,

$$\rho \left[\frac{\partial}{\partial t} (\phi \langle \bar{\mathbf{u}} \rangle^i) + \nabla \cdot (\phi \langle \bar{\mathbf{u}}\bar{\mathbf{u}} \rangle^i) \right]$$
$$= -\nabla(\phi \langle \bar{p} \rangle^i) + \mu \nabla^2 (\phi \langle \bar{\mathbf{u}} \rangle^i) + \nabla \cdot (-\rho \phi \langle \overline{\mathbf{u}'\mathbf{u}'} \rangle^i) + \overline{\mathbf{R}} \tag{2}$$

As usually done when treating turbulence with statistical tools, the correlation $-\rho \overline{\mathbf{u}'\mathbf{u}'}$ appears after application of the time-average operator to the local instantaneous NS equation. Applying further the volume-average procedure to the entire momentum equation (see [14] for details), results in the term $-\rho \phi \langle \overline{\mathbf{u}'\mathbf{u}'} \rangle^i$ of (2). This term is here recalled as the macroscopic Reynolds stress tensor (MRST). In addition, $\overline{\mathbf{R}}$ in (2) represents the time-mean total drag per unit volume acting on the fluid by the action of the porous structure. A common model for it is known as the Darcy–Forchheimer extended model and is given by:

$$\overline{\mathbf{R}} = -\left[\frac{\mu \phi}{K} \bar{\mathbf{u}}_D + \frac{c_F \phi \rho |\bar{\mathbf{u}}_D| \bar{\mathbf{u}}_D}{\sqrt{K}} \right] \tag{3}$$

where the constant c_F is known in the literature as the nonlinear Forchheimer coefficient.

Then, making use again of the expression $\bar{\mathbf{u}}_D = \phi \langle \bar{\mathbf{u}} \rangle^i$ and (3), Eq. (2) can be rewritten as,

$$\rho \left[\frac{\partial \bar{\mathbf{u}}_D}{\partial t} + \nabla \cdot \left(\frac{\bar{\mathbf{u}}_D \bar{\mathbf{u}}_D}{\phi} \right) \right]$$
$$= -\nabla(\phi \langle \bar{p} \rangle^i) + \mu \nabla^2 \bar{\mathbf{u}}_D + \nabla \cdot (-\rho \phi \langle \overline{\mathbf{u}'\mathbf{u}'} \rangle^i)$$
$$- \left[\frac{\mu \phi}{K} \bar{\mathbf{u}}_D + \frac{c_F \phi \rho |\bar{\mathbf{u}}_D| \bar{\mathbf{u}}_D}{\sqrt{K}} \right] \tag{4}$$

Further, a model for the MRST in analogy with the Boussinesq concept for clear fluid can be written as:

$$-\rho \phi \langle \overline{\mathbf{u}'\mathbf{u}'} \rangle^i = \mu_{t_\phi} 2 \langle \overline{\mathbf{D}} \rangle^v - \frac{2}{3} \phi \rho \langle k \rangle^i \mathbf{I} \tag{5}$$

where

$$\langle \overline{\mathbf{D}} \rangle^v = \frac{1}{2} \left[\nabla(\phi \langle \bar{\mathbf{u}} \rangle^i) + [\nabla(\phi \langle \bar{\mathbf{u}} \rangle^i)]^T \right] \tag{6}$$

is the macroscopic deformation tensor, $\langle k \rangle^i$ is the intrinsic average for k and μ_{t_ϕ} is the macroscopic turbulent viscosity. The macroscopic turbulent viscosity, μ_{t_ϕ}, used in (5) is modeled similarly to the case of clear fluid flow and a proposal for it was presented in [14] as,

$$\mu_{t_\phi} = \rho c_\mu \langle k \rangle^{i^2} / \langle \varepsilon \rangle^i \tag{7}$$

2.2. Macroscopic equations for $\langle k \rangle^i$ and $\langle \varepsilon \rangle^i$

Transport equations for $\langle k \rangle^i = \overline{\langle \mathbf{u}' \cdot \mathbf{u}' \rangle}^i / 2$ and $\langle \varepsilon \rangle^i = \mu \overline{\langle \nabla \mathbf{u}' : (\nabla \mathbf{u}')^T \rangle}^i / \rho$ in their so-called high Reynolds number form are proposed in [14] as:

$$\rho \left[\frac{\partial}{\partial t} (\phi \langle k \rangle^i) + \nabla \cdot (\bar{\mathbf{u}}_D \langle k \rangle^i) \right]$$
$$= \nabla \cdot \left[\left(\mu + \frac{\mu_{t_\phi}}{\sigma_k} \right) \nabla(\phi \langle k \rangle^i) \right] + P^i + G^i - \rho \phi \langle \varepsilon \rangle^i \tag{8}$$

where $P^i = -\rho \langle \overline{\mathbf{u}'\mathbf{u}'} \rangle^i : \nabla \bar{\mathbf{u}}_D$, $G^i = c_k \rho \frac{\phi \langle k \rangle^i |\bar{\mathbf{u}}_D|}{\sqrt{K}}$ and

$$\rho \left[\frac{\partial}{\partial t} (\phi \langle \varepsilon \rangle^i) + \nabla \cdot (\bar{\mathbf{u}}_D \langle \varepsilon \rangle^i) \right]$$
$$= \nabla \cdot \left[\left(\mu + \frac{\mu_{t_\phi}}{\sigma_\varepsilon} \right) \nabla(\phi \langle \varepsilon \rangle^i) \right]$$
$$+ c_1 P^i \frac{\langle \varepsilon \rangle^i}{\langle k \rangle^i} + c_2 \frac{\langle \varepsilon \rangle^i}{\langle k \rangle^i} (G^i - \rho \phi \langle \varepsilon \rangle^i) \tag{9}$$

where c_1, c_2 and c_k are constants, P^i is the production rate of $\langle k \rangle^i$ due to gradients of $\bar{\mathbf{u}}_D$ and G^i the generation rate of the intrinsic average of k due to the action of the porous matrix. Eqs. (8) and (9) could also have been written in terms of volume or Darcy values using the equalities $\langle k \rangle^v = \phi \langle k \rangle^i$ and $\langle \varepsilon \rangle^v = \phi \langle \varepsilon \rangle^i$, respectively. However, for the sake of simplicity and coherence with the majority of publications on this subject, transport equations for $\langle k \rangle^i$ and $\langle \varepsilon \rangle^v$ are here employed.

2.3. Interface and "jump" conditions

The equation proposed by [6,7] for describing the stress jump at the interface has been modified in [13,32] in order to consider turbulent flow, in the form,

$$(\mu_{eff} + \mu_{t_\phi}) \frac{\partial \bar{u}_{D_p}}{\partial y} \bigg|_{Porous\,medium} - (\mu + \mu_t) \frac{\partial \bar{u}_{D_p}}{\partial y} \bigg|_{Clear\,fluid}$$
$$= (\mu + \mu_t) \frac{\beta}{\sqrt{K}} \bar{u}_{D_p} \bigg|_{interface} \tag{10}$$

where u_{D_p} is the Darcy velocity component parallel to the interface, μ_{eff} is the effective viscosity for the porous region, which is given by $\mu_{\text{eff}} = \mu/\phi$ according to [6,7], and β is an adjustable coefficient that accounts for the stress jump at the interface.

It is interesting to note that Eq. (10) comes from the sole extension, to turbulent flows, of the proposal in [6,7], which for laminar flow reads,

$$\mu_{\text{eff}} \frac{\partial u_{D_p}}{\partial y}\Big|_{\text{Porous medium}} - \mu \frac{\partial u_{D_p}}{\partial y}\Big|_{\text{Clear fluid}} = \mu \frac{\beta}{\sqrt{K}} u_{D_p}\Big|_{\text{interface}}$$

(11)

Local instantaneous velocities in (11) were replaced by time-averaged values and a "total" diffusivity is used as a substitute for the molecular diffusivity. Physically, Eq. (10) is guided by the same arguments that standard well-known "eddy-diffusivity" models rely on, which is the use of a diffusion-like expression having, instead, gradients of time-averaged values and a total (laminar plus turbulent) viscosity. Although it is recognized that Eq. (10) needs further validation against experimental values, its application herein is assumed in lieu of better information.

Continuity of velocity, pressure, statistical variables and their fluxes across the interface are given by (see [32] for details),

$$\bar{\mathbf{u}}_D\big|_{\text{Porous medium}} = \bar{\mathbf{u}}_D\big|_{\text{Clear fluid}}$$

(12)

$$\langle \bar{p} \rangle^i\big|_{\text{Porous medium}} = \langle \bar{p} \rangle^i\big|_{\text{Clear fluid}}$$

(13)

$$\langle k \rangle^v\big|_{\text{Porous medium}} = \langle k \rangle^v\big|_{\text{Clear fluid}}$$

(14)

$$\left(\mu + \frac{\mu_{t_\phi}}{\sigma_k}\right)\frac{\partial \langle k \rangle^v}{\partial y}\Big|_{\text{Porous medium}} = \left(\mu + \frac{\mu_t}{\sigma_k}\right)\frac{\partial \langle k \rangle^v}{\partial y}\Big|_{\text{Clear fluid}}$$

(15)

$$\langle \varepsilon \rangle^v\big|_{\text{Porous medium}} = \langle \varepsilon \rangle^v\big|_{\text{Clear fluid}}$$

(16)

$$\left(\mu + \frac{\mu_{t_\phi}}{\sigma_\varepsilon}\right)\frac{\partial \langle \varepsilon \rangle^v}{\partial y}\Big|_{\text{Porous medium}} = \left(\mu + \frac{\mu_t}{\sigma_\varepsilon}\right)\frac{\partial \langle \varepsilon \rangle^v}{\partial y}\Big|_{\text{Clear fluid}}$$

(17)

Eqs. (12) and (13) were also proposed by [6] whereas relationships (14)–(17) were used by [44].

In Silva and de Lemos [32], no "jump" condition was considered when treating the diffusion flux of $\langle k \rangle^v$ across the interface, as can be seen by Eq. (15). In [43], such discontinuity in the diffusion transport of $\langle k \rangle^v$ between the two media was first considered. Such "jump" might be a model for accounting for interface roughness or be a way to comply with irregular interfaces. In addition, it can also be seen as an accommodation of the fact that close to the interface the permeability K attains higher values than those used within the porous substrate. For that, the interface condition of de Lemos [43] is here applied,
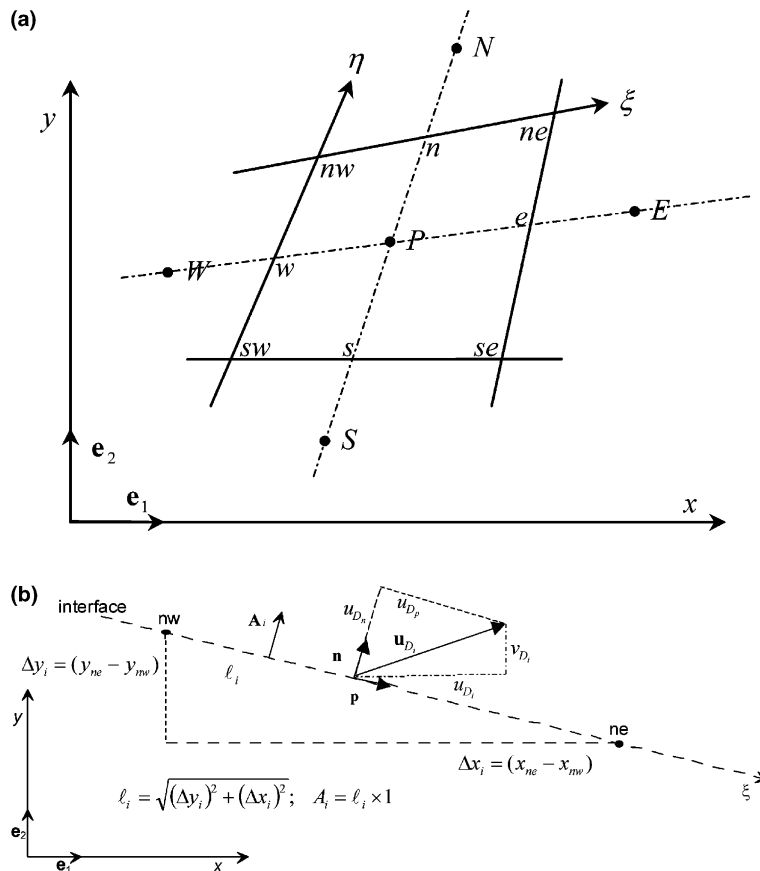
Fig. 2. Notation for: (a) control volume discretization, (b) interface treatment.

$$\left(\mu_{\text{eff}} + \frac{\mu_{\text{t}_\phi}}{\sigma_k}\right)\frac{\partial\langle k\rangle^v}{\partial y}\bigg|_{\text{Porous medium}} - \left(\mu + \frac{\mu_{\text{t}}}{\sigma_k}\right)\frac{\partial\langle k\rangle^v}{\partial y}\bigg|_{\text{Clear fluid}}$$

$$= (\mu + \mu_{\text{t}})\frac{\beta}{\sqrt{K}}\langle k\rangle^v\bigg|_{\text{interface}} \qquad (18)$$

instead of Eq. (15). Condition (18) is imposed along the interface shown in Fig. 2b.

Eq. (18) results from the following reasoning. If interface condition (10) is written in its instantaneous form, it gives,

$$(\mu_{\text{eff}} + \mu_{\text{t}_\phi})\frac{\partial u_{\text{D}_\text{p}}}{\partial y}\bigg|_{\text{Porous medium}} - (\mu + \mu_{\text{t}})\frac{\partial u_{\text{D}_\text{p}}}{\partial y}\bigg|_{\text{Clear fluid}}$$

$$= (\mu + \mu_{\text{t}})\frac{\beta}{\sqrt{K}}u_{\text{D}_\text{p}}\bigg|_{\text{interface}} \qquad (19)$$

Assuming that the component of the Darcy velocity along the interface varies with time, a standard time decomposition for it can be written as $u_{\text{D}_\text{p}} = \bar{u}_{\text{D}_\text{p}} + u'_{\text{D}_\text{p}}$. Next, considering that only velocities fluctuate in time, subtracting (10) from (19) results in the following relationship for the fluctuating interface velocity u'_{D_p},

$$(\mu_{\text{eff}} + \mu_{\text{t}_\phi})\frac{\partial u'_{\text{D}_\text{p}}}{\partial y}\bigg|_{\text{Porous medium}} - (\mu + \mu_{\text{t}})\frac{\partial u'_{\text{D}_\text{p}}}{\partial y}\bigg|_{\text{Clear fluid}}$$

$$= (\mu + \mu_{\text{t}})\frac{\beta}{\sqrt{K}}u'_{\text{D}_\text{p}}\bigg|_{\text{interface}} \qquad (20)$$

Taking now the scalar product of u'_{D_p} and Eq. (20), one gets,

$$(\mu_{\text{eff}} + \mu_{\text{t}_\phi})\frac{\partial((u'_{\text{D}_\text{p}} \cdot u'_{\text{D}_\text{p}})/2)}{\partial y}\bigg|_{\text{Porous medium}}$$

$$- (\mu + \mu_{\text{t}})\frac{\partial((u'_{\text{D}_\text{p}} \cdot u'_{\text{D}_\text{p}})/2)}{\partial y}\bigg|_{\text{Clear fluid}}$$

$$= (\mu + \mu_{\text{t}})\frac{\beta}{\sqrt{K}}((u'_{\text{D}_\text{p}} \cdot u'_{\text{D}_\text{p}})/2)\bigg|_{\text{interface}} \qquad (21)$$

If one now apply the time-averaging operation to Eq. (21) and for flows mostly parallel to the interface approximate the turbulence kinetic energy as $\langle k\rangle^v \approx \overline{u'_{\text{D}_\text{p}} \cdot u'_{\text{D}_\text{p}}}/2$, condition (18) is recovered after introducing the constant σ_k on the left hand side of (21).

One should further mention that a different coefficient β and constant σ_k, on the right hand side of (18), might be both necessary to accommodate real engineering flows over porous substrates. Proposition (18), as such, should be regarded as a first step towards realistic modeling subjected to improvements as experimental data on macroscopic interfaces become available.

3. Numerical details

Fig. 2a shows a general control volume in a two-dimensional configuration. The faces of the volume are formed by lines of constant coordinates η–ξ. The work in [31] was set up for solving one-dimensional laminar

flows in the geometry of Fig. 1 and employed the spatially periodic boundary condition along the x-coordinate. This was done in order to simulate fully developed flow. The spatially periodic condition was implemented by running the 2D solution repetitively, until outlet profiles in $x = L$ matched those at the inlet ($x = 0$). Details on the methodology here employed for simulating fully developed flow using a two-dimensional numerical tool and the periodic condition along the x-direction can be found in [15–17].

Grid independence studies were conducted by Silva and de Lemos [32] and for more than 40 nodal points in the cross-stream direction, the solution was essentially grid independent. Twenty points were allocated within each channel medium (porous and clear). Such optimal grid had points concentrated around the interface and close to the impermeable wall at the top (see Fig. 1a) giving for the control volumes a variable height Δx. Further, as also explained in Silva and de Lemos [32], for all cases considered a total of 50 nodes in the axial direction was found to suffice, leading to computational nodes of constant width $\Delta y = L/50$.

In Silva and de Lemos [31], the discretization methodology used for including the jump condition in the numerical solutions was discussed. For that, only brief comments about the numerical procedure are here made. Also, details of the discretization of the terms on the left of (10) can be found in Pedras and de Lemos [15]. Furthermore, information on the discretization of the right of (10) appears in Silva and de Lemos [31] where more particulars can be found. Here, attention is focused on the numerical treatment of (18), whose discretization followed the nomenclature shown in Fig. 2a.

For steady-state, a general form of the discrete equations for a general variable φ becomes,

$$I_{\text{e}} + I_{\text{w}} + I_{\text{n}} + I_{\text{s}} = S_{\varphi} \qquad (22)$$

where I_{e}, I_{w}, I_{n} and I_{s} are the fluxes of φ at faces *east*, *west*, *north* and *south* of the control volume of Fig. 2a, respectively, and S_{φ} is a source term. Here, all computations were carried out until normalized residues of the algebraic equations were brought down to 10^{-7}.

Fig. 2b shows details of the interface dividing two control volumes, one being located in the porous region and the other lying in the clear fluid. The computational grid based on generalized coordinate system η–ξ is such that the interface coincides with a line of constant η, extending itself along the ξ coordinate. In this arrangement, the interface between the two neighbor volumes, each one located on each side of the interface, belongs to both faces of the two volumes. Thus, according to Fig. 2b, $\bar{\mathbf{u}}_{\text{D}_\text{i}}$ is the Darcy velocity at the interface and $\bar{\mathbf{u}}_{\text{D}_\text{p}}$ its component parallel to the interface.

Further, in Fig. 2b one can identify all variables located at the interface. The modulus of the macroscopic interfacial area can be expressed as,

$$| \mathbf{A}_i | = A_i = \ell_i \times 1 = \sqrt{(x_{ne} - x_{nw})^2 + (y_{ne} - y_{nw})^2} \qquad (23)$$

Integrating the left hand side of (18) over the macroscopic interfacial area A_i, and considering further constant $\langle k \rangle^i$ and constant properties prevailing over the integration area, one has,

$$I_i^{\beta_k} = \int_{A_i} (\mu + \mu_t) \frac{\beta}{\sqrt{K}} \langle k \rangle^v \Big|_i \mathrm{d}A_i \approx (\mu + \mu_t)_i \frac{\beta}{\sqrt{K}} \langle k \rangle^v \Big|_i A_i \quad (24)$$

or

$$\begin{aligned} I_i^{\beta_k} &\approx (\mu + \mu_t)_i \frac{\beta}{\sqrt{K}} \langle k \rangle^v \Big|_i A_i \\ &= (\mu + \mu_t)_i \frac{\beta}{\sqrt{K}} \langle k \rangle^v \ell_i \\ &= (\mu + \mu_t)_i \frac{\beta}{\sqrt{K}} \langle k \rangle^v \sqrt{(x_{ne} - x_{nw})^2 + (y_{ne} - y_{nw})^2} \end{aligned} \quad (25)$$

The term on the right of (25) is added to the discretized k-equation components when the nodal point in question has a face coincident with the interface. For ease of implementation, these additional terms are treated in an explicit form and are added to the right hand side of (22).

4. Results and discussion

The flow in Fig. 1 was computed with the set of equations (4), (8) and (9) with additional constitutive equation (5) and the macroscopic Kolmogorov–Prandtl expression (7). The wall function approach was used for treating the flow close to the wall. Grid independence studies were conducted in Silva and de Lemos [31] and, for more than 40 nodal points in the cross-stream direction, the solution was essentially grid independent. One should emphasize that the numerical methodology here considered was focused on two-dimensional flows, so that simulating the
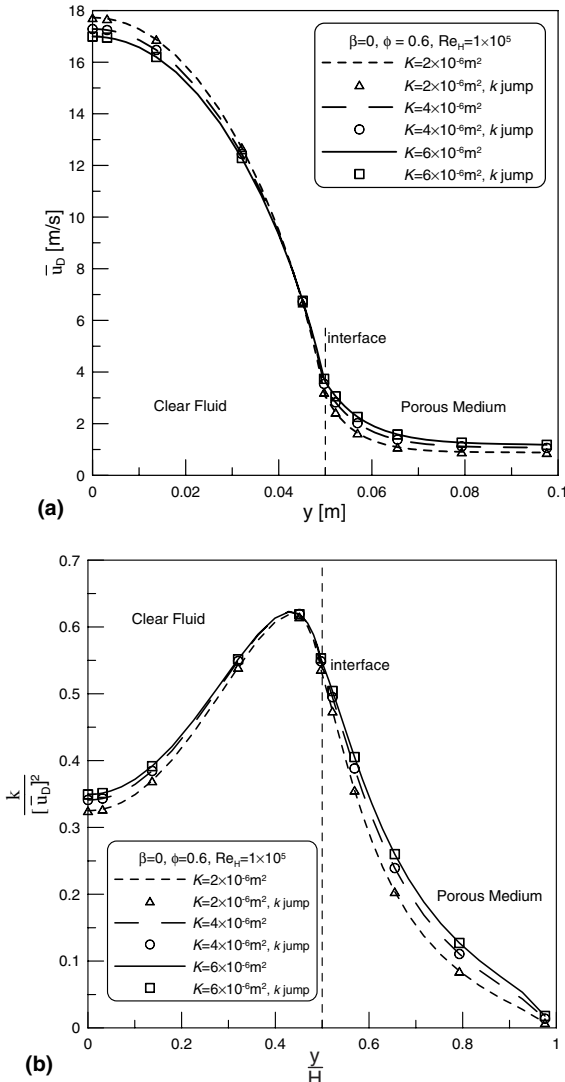
Fig. 3. Calculations using Eq. (15) (lines) compared with simulations with expression (18) (symbols) and $\beta = 0$: (a) mean field, (b) turbulent field.
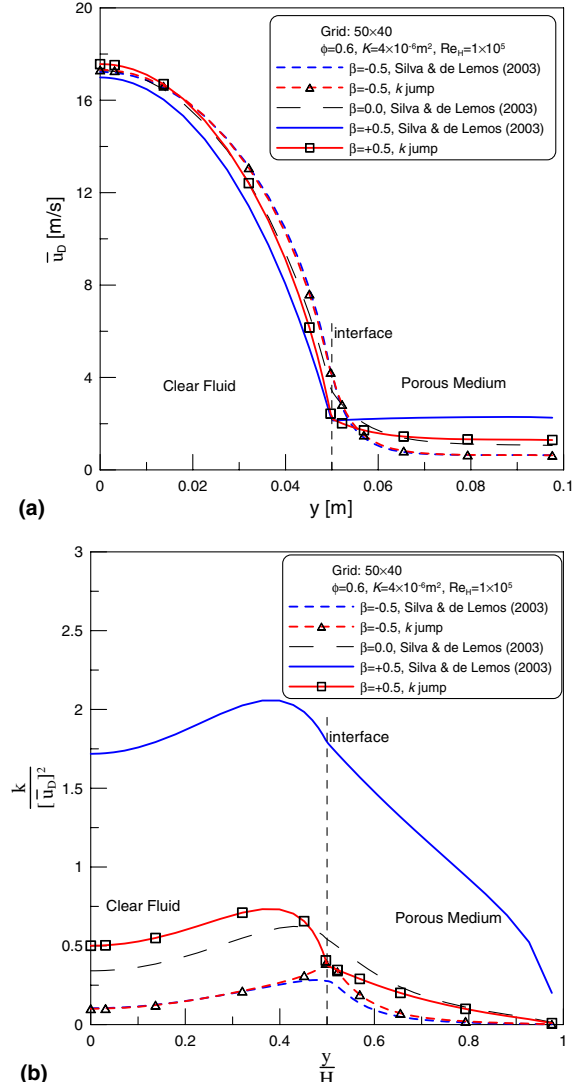
Fig. 4. Effect of jump conditions on mean and turbulent fields: (a) mean velocity **u**, (b) non-dimensional turbulent kinetic energy.

fully developed situation shown in the figure required the used of nodal points along the axial direction as well as the employment of the spatially periodic condition mentioned earlier. For all runs here studied, a total of 50 nodes in the axial direction was found to suffice. It is also important to note that the sign of coefficient β is expression (10) and (18) depend on the orientation of the y-axis in relation to the porous layer location. Here, the same orientation given by Kuznetzov [8–10] was used, which considers the porous layer at the top of the channel with its normal pointing towards the minus y-direction. As such, coherent computations for laminar flow [31] were obtained. As mentioned, grid independence studies were carried out by Silva and de Lemos [31] indicating the proper number of nodal points used around the interface. There, the authors correctly reproduced, with their numerical tool, the bound-

ary layers around the interface proposed by the analytical study of Kuznetzov [8–10]. Also for the case of turbulent flow the number of grid point used seems to be appropriate.

In order to check for the correctness of computer code developed, two results were compared. Calculations applying Eq. (15) used in Silva and de Lemos [32] were compared with simulation with (18) setting $\beta = 0$. Fig. 3 correctly shows superposition of results for the mean and turbulent fields, indicating proper computer implementation of the diffusion-jump model for the k-equation.

Fig. 4a presents numerical solutions for varying from -0.5 to 0.5 for a fixed porosity $\phi = 0.6$, permeability $K = 4 \times 10^{-4} \text{ m}^2$ and $Re_H = 1 \times 10^5$. Results are compared with those by Silva and de Lemos [32], who used interface conditions (10) and (15) for the mean and turbulent fields,
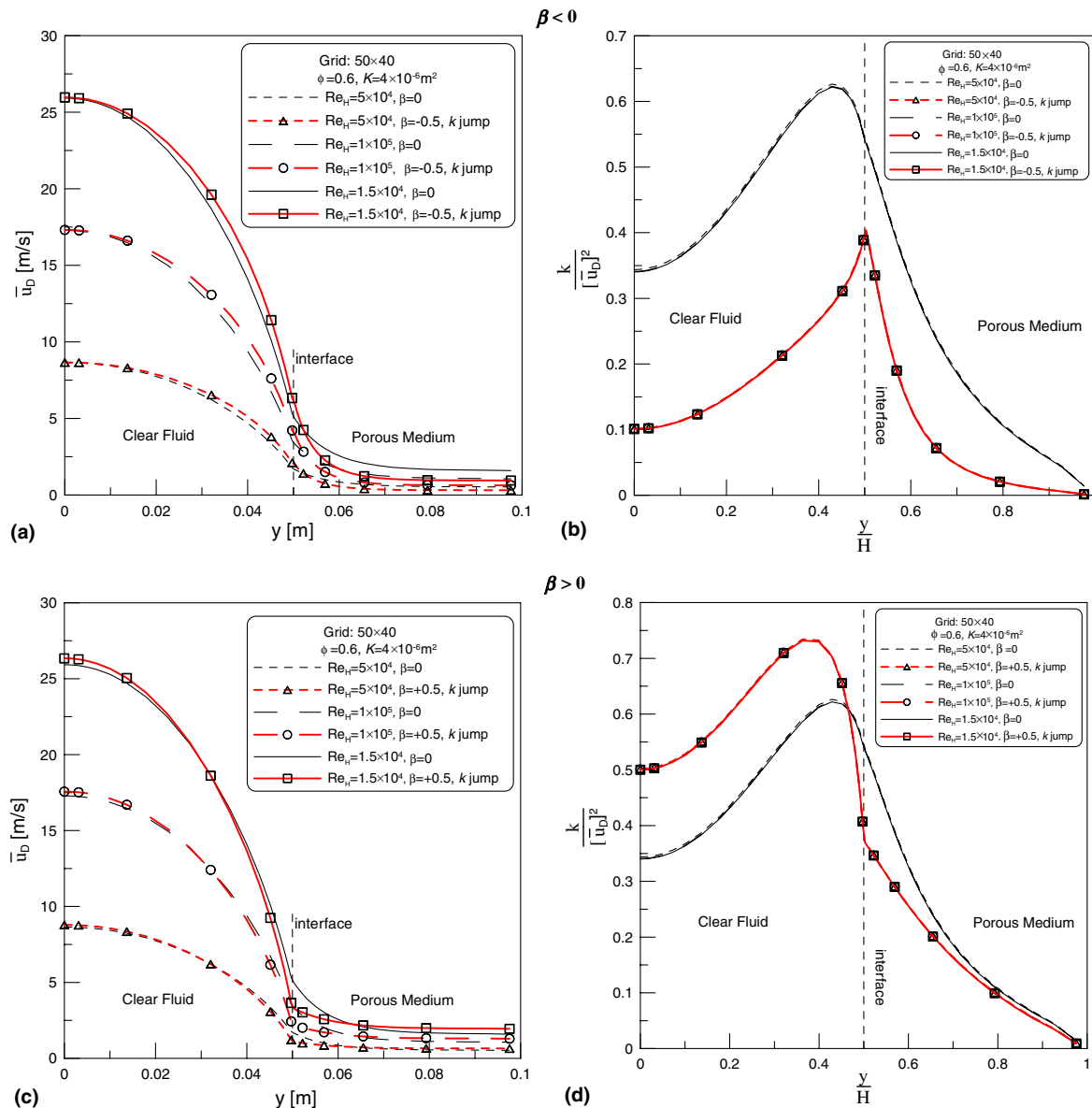
Fig. 5. Effect of Reynolds number, Re_H, on macroscopic field. $\beta < 0$: (a) mean velocity, (b) turbulent kinetic energy; $\beta > 0$: (c) mean velocity, (d) turbulent kinetic energy.
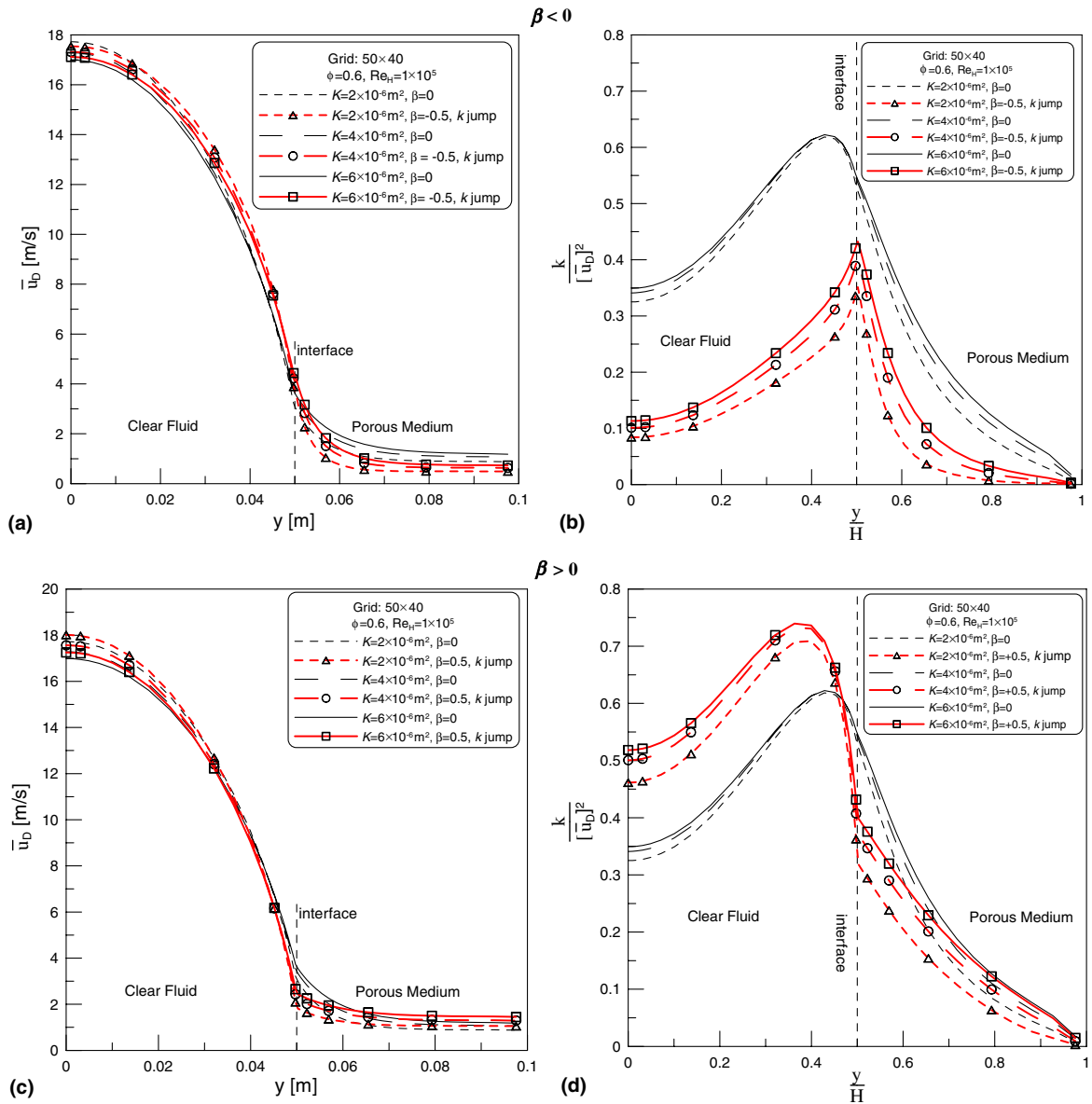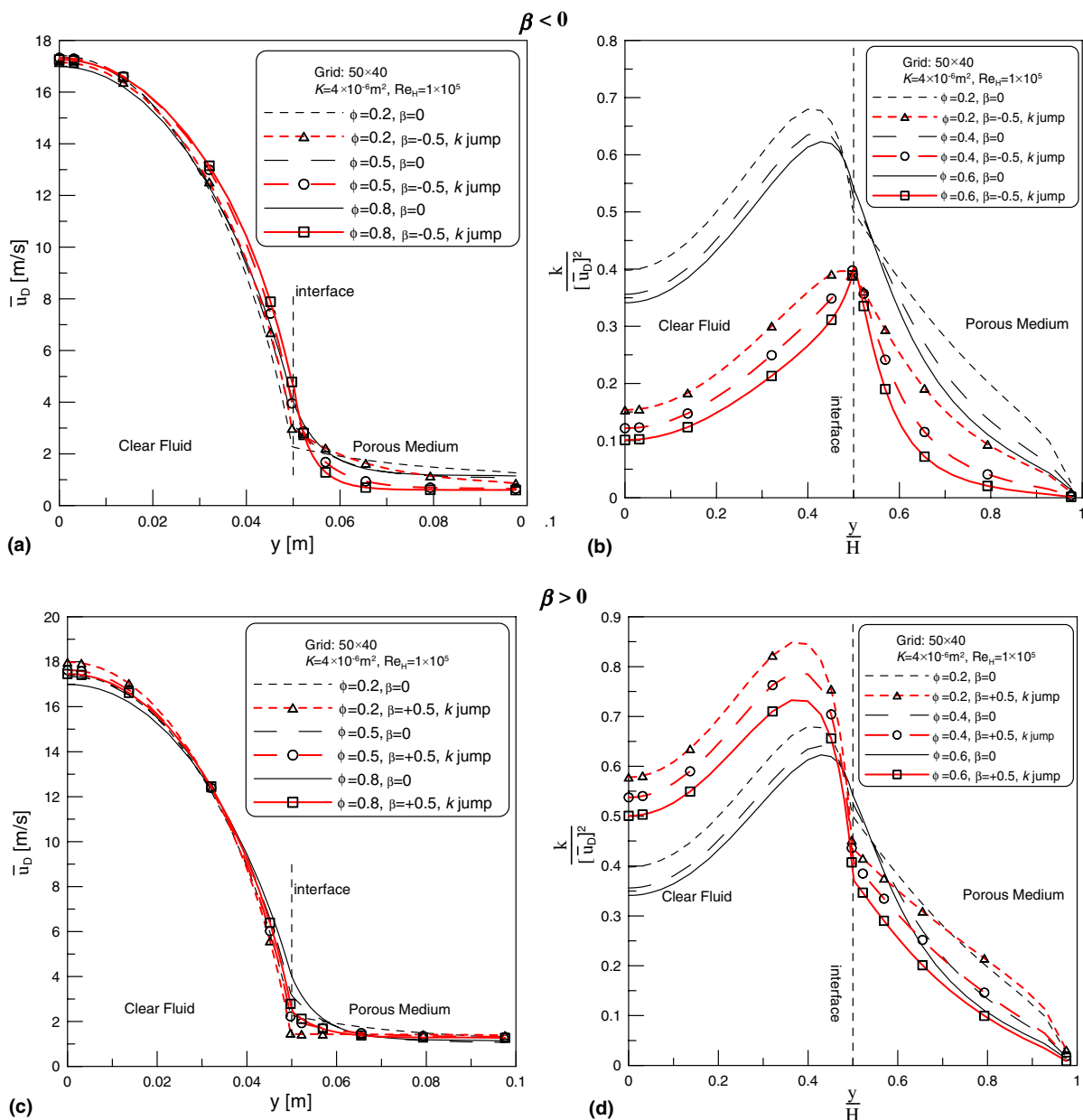
Fig. 6. Effect of permeability, K, on macroscopic field. $\beta < 0$: (a) mean velocity, (b) turbulent kinetic energy; $\beta > 0$: (c) mean velocity, (d) turbulent kinetic energy.

respectively. When condition (18) is used in place of (15), profiles for $\bar{u}_D$ change substantially as the factor β is varied from a smooth variation across the interface for a negative β (small dashed line without symbols, Fig. 4a) to an abrupt change in the velocity profiles when $\beta > 0$ (solid line without symbols, Fig. 4a). For positive β values, the Darcy velocity $\bar{u}_D$ is slightly higher inside the permeable structure than at the interface, indicating that flow resistance at this position would be higher than everywhere across the porous layer [43]. This unrealistic result is not obtained when condition (18) is applied for $\langle k \rangle^v$ (solid line with symbols, Fig. 4a). In this case, velocities close to the wall region are higher than for $\beta = 0$ ($y > 0.064$ m, large dashed line), but around the interface no such minimum in the value of $\bar{u}_D$ is observed. For $\beta < 0$ (small dashed lines) no sub-

stantial difference in the calculated profiles, with and without a jump condition for $\langle k \rangle^v$, is observed.

Distributions for turbulent kinetic energy as a function of the interface boundary condition are shown in Fig. 4b. The clear separation for the two distributions for positive and negative values of β calculated by Silva and de Lemos [32] (solid and small dashed lines, without symbols) is not seen when interface condition (18) is applied (solid and small dashed curves, with symbols). The region of maximum turbulent kinetic energy is within the clear flow ($y < 0.05$ m) for $\beta > 0$ (solid line with symbols), whereas the use of a negative value for the jump parameter causes a peak for $\langle k \rangle^v$ at the interface (dashed curve with symbols). If one compares with experimental values by [39] (not shown here), one can conclude that models with

negative β values are closer to representing reality for turbulent flow around a porous medium.

The effect of Re_H is shown in Fig. 5. Plots on the left (a, c) are for mean velocity whereas curves on the right of the figure (b, d) details the behavior of the turbulent filed. Also, drawings on the top (a, b) were calculated for $\beta < 0$ whereas figures on the bottom (c, d) used positive values of β. The mean velocity profiles in Fig. 5a and c confirms the increasing mass flow rate within either the porous material or the clear passage as Re_H increases. In Fig. 5b and d the collapse of curves for the turbulent kinetic energy divided by the mean mechanical energy shows that, for the range of Re_H here analyzed, the percentage of energy trans-

formed into turbulence remains the same, regardless of the diffusion-jump model used. The most striking feature in Fig. 5 is the different response, in the turbulence field (b, d), when using values for β of different sign. Negative values for β (Fig. 5b) indicate that the peaks in the curves lie lower than when no jump condition is used, and that this peak is at the interface. On the other hand, for a positive β, the levels of k are higher than if no jump condition is applied. In addition, the peaks are moved towards the center of the channel. The behavior of the curves is associated with corresponding mean velocity profiles. Within the clear fluid, the production of turbulent kinetic energy is known to be dictated by gradients of the mean velocity (P^i on

Fig. 7. Effect of porosity, ϕ, on macroscopic field. $\beta < 0$: (a) mean velocity, (b) turbulent kinetic energy; $\beta > 0$: (c) mean velocity, (d) turbulent kinetic energy.

the right of (8)) whereas inside the permeable structure, the model of [14] proposes a factor proportional to $\bar{\mathbf{u}}_D$ as a generating mechanism for k (G^i in Eq. (8)).

Fig. 6 shows the effect of the permeability K on both the mean and statistical fields. Plots a–d follow the same convention described in Fig. 5. The figure indicates that the greater the permeability, more flow crosses the porous substratum located in the region $0.5 < y/H < 1$ (Fig. 6a–c). The curves representing the statistical field in Fig. 6b–d show that the levels of k increase with increasing K. As more fluid flows in less resistant media, more mean mechanical energy is transformed into turbulence increasing the overall level of k.

Finally, Fig. 7 investigates the effect of the value of ϕ on the behavior of the mean and turbulent fields, here also following the same convention established when presenting Fig. 5 (plots a–d). For the mean field (a,c), one can note that close to $y/H = 0.5$ the greater the porosity, the higher the velocity at the interface and the greater the mass flow rate closer to this region. At the center of the channel, the velocity decreases in order to keep the imposed mass flow rate the same. It is interesting to observe that since the overall mass flow rate is forced to be constant, instead of the overall pressure loss along the channel, an enhancement of the mass flow rate along the porous bed in the interface region is compensated by a slight reduction on local velocities close to the wall. Fig. 7b–d shows corresponding curves for the behavior of the turbulent kinetic energy. Values of k present a slight reduction as ϕ is incremented. Lower values for the turbulence level within the porous layer are coherent with the model of Eq. (8) for the extra generation rate due to the porous matrix. As said, this extra G^i term (third on the right of (8)) was modeled as proportional to $\bar{\mathbf{u}}_D$ and, inside the porous layer, the mean Darcy velocity is reduced as ϕ increases.

Ultimately, results in Figs. 5–7 indicates that for flows where models with $\beta < 0$ are suitable, a smaller portion of the mean mechanical energy of the flow is converted into turbulence. Results herein might be useful to environmentalists and engineers analyzing important natural and engineering flows. Although in the porous substrate mean velocity profiles are flatter, reducing the production rate P^i, the generating mechanism G^i is proportional to $\bar{\mathbf{u}}_D$, increases the overall value of k. In the clear fluid, steeper gradients in the fluid layer also contributes for increasing the value of the turbulent kinetic energy. Then, either by P^i in the clear fluid or by G^i in the porous layer, turbulent kinetic energy is generated at a faster rate for positive values of β.

5. Concluding remarks

Numerical solutions for turbulent flow in composite channels were obtained for different values of Re_H, ϕ, K and β parameters. Results were compared with previous computations by Silva and de Lemos [32], which did not include a diffusion jump for k. Inclusion of such term resulted

in qualitatively different profiles for the turbulence kinetic energy, ultimately indicating a different portion of the available mechanical energy that is converted into turbulence. Although simulations were presented for one-dimensional flows, the implementation herein was done for two-dimensional situations and carried out on a generalized coordinate system. Future applications of the model herein may be useful on the determining of the overall exchange rates of energy and mass transport across a interface between a porous medium and a clear region.

References

[1] X.Y. Zhou, J.C.F. Pereira, A multidimensional model for simulating vegetation fire spread using a porous media sub-model, Fire Mater. 24 (2000) 37–43.

[2] M.R. Hoffmann, Application of a simple space-time averaged porous media model to flow in densely vegetated channels, J. Porous Media 7 (3) (2004) 183–191.

[3] S.N. Lane, R.J. Hardy, Porous rivers: a new way of conceptualizing and modeling river and floodplain flows? in: D. Ingham, I. Pop (Eds.), Transport Phenomena in Porous Media II, first ed., Pergamon Press, 2002, pp. 425–449 [Chapter 16].

[4] M. Prithiviraj, M.J. Andrews, Three-dimensional numerical simulation of steel-and-tube heat exchanger. Part I—Foundation and fluid mechanics, Numer. Heat Transfer A—Appl. 33 (1998) 799–816.

[5] W.T. Sha, A new porous-media approach for thermal–hydraulic analysis, Trans. ANS 39 (1981) 510–512.

[6] J.A. Ochoa-Tapia, S. Whitaker, Momentum transfer at the boundary between a porous medium and a homogeneous fluid. I—Theoretical development, Int. J. Heat Mass Transfer 38 (1995) 2635–2646.

[7] J.A. Ochoa-Tapia, S. Whitaker, Momentum transfer at the boundary between a porous medium and a homogeneous fluid. II—Comparison with experiment, Int. J. Heat Mass Transfer 38 (1995) 2647–2655.

[8] A.V. Kuznetsov, Analytical investigation of the fluid flow in the interface region between a porous medium and a clear fluid in channels partially filled with a porous medium, Int. J. Heat Fluid Flow 12 (1996) 269–272.

[9] A.V. Kuznetsov, Influence of the stresses jump condition at the porous-medium/clear-fluid interface on a flow at a porous wall, Int. Commun. Heat Mass Transfer 24 (1997) 401–410.

[10] A.V. Kuznetsov, Fluid mechanics and heat transfer in the interface region between a porous medium and a fluid layer: a boundary layer solution, J. Porous Media 2 (3) (1999) 309–321.

[11] S. Whitaker, Advances in theory of fluid motion in porous media, Indust. Eng. Chem. 61 (1969) 14–28.

[12] W.G. Gray, P.C.Y. Lee, On the theorems for local volume averaging of multiphase system, Int. J. Multiphase Flow 3 (1977) 333–340.

[13] M.J.S. de Lemos, M.H.J. Pedras, Simulation of turbulent flow through hybrid porous medium-clear fluid domains, in: Proc. of IMECE2000—ASME—Int. Mech. Eng. Congr., ASME-HTD-366-5, ISBN 0-7918-1908-6, Orlando, FL, 2000, pp. 113–122.

[14] M.H.J. Pedras, M.J.S. de Lemos, Macroscopic turbulence modeling for incompressible flow through undeformable porous media, Int. J. Heat Mass Transfer 44 (6) (2001) 1081–1093.

[15] M.H.J. Pedras, M.J.S. de Lemos, Simulation of turbulent flow in porous media using a spatially periodic array and a low Re

two-equation closure, Numer. Heat Transfer A—Appl. 39 (1) (2001) 35–59.

[16] M.H.J. Pedras, M.J.S. de Lemos, On mathematical description and simulation of turbulent flow in a porous medium formed by an array of elliptic rods, ASME J. Fluids Eng. 123 (4) (2001) 941–947.

[17] M.H.J. Pedras, M.J.S. de Lemos, Computation of turbulent flow in porous media using a low Reynolds k–ε model and an infinite array of transversally displaced elliptic rods, Numer. Heat Transfer A—Appl. 43 (6) (2003) 585–602.

[18] M.H.J. Pedras, M.J.S. de Lemos, On volume and time averaging of transport equations for turbulent flow in porous media, ASME-FED, vol. 248, Paper FEDSM99-7273, ISBN 0-7918-1961-2, 1999.

[19] M.H.J. Pedras, M.J.S. de Lemos, On the definition of turbulent kinetic energy for flow in porous media, Int. Commun. Heat Mass Transfer 27 (2) (2000) 211–220.

[20] F.D. Rocamora Jr., M.J.S. de Lemos, Analysis of convective heat transfer for turbulent flow in saturated porous media, Int. Commun. Heat Mass Transfer 27 (6) (2000) 825–834.

[21] M.J.S. de Lemos, M.H.J. Pedras, Recent mathematical models for turbulent flow in saturated rigid porous media, ASME J. Fluids Eng. 123 (4) (2001) 935–940.

[22] M.J.S. de Lemos, E.J. Braga, Modeling of turbulent natural convection in saturated rigid porous media, Int. Commun. Heat Mass Transfer 30 (5) (2003) 615–624.

[23] M.J.S. de Lemos, M.S. Mesquita, Turbulent mass transport in saturated rigid porous media, Int. Commun. Heat Mass Transfer 30 (1) (2003) 105–113.

[24] M.J.S. de Lemos, L.A. Tofaneli, Modeling of double-diffusive turbulent natural convection in porous media, Int. J. Heat Mass Transfer 47 (19–20) (2004) 4221–4231.

[25] E.J. Braga, M.J.S. de Lemos, Turbulent natural convection in a porous square cavity computed with a macroscopic k–ε model, Int. J. Heat Mass Transfer 47 (26) (2004) 5639–5650.

[26] E.J. Braga, M.J.S. de Lemos, Heat transfer in enclosures having a fixed amount of solid material simulated with heterogeneous and homogeneous models, Int. J. Heat Mass Transfer 48 (23–24) (2005) 4748–4765.

[27] E.J. Braga, M.J.S. de Lemos, Laminar natural convection in cavities filled with circular and square rods, Int. Commun. Heat Mass Transfer, in press.

[28] F.D. Rocamora Jr., M.J.S. de Lemos, Laminar recirculating flow and heat transfer in hybrid porous medium-clear fluid computational domains, in: Proc. of 34th ASME-National Heat Transfer Conference (on CD-ROM), ASME-HTD-I463CD, Paper NHTC2000-12317, ISBN 0-7918-1997-3, Pittsburgh, PA, 2000.

[29] F.D. Rocamora Jr., M.J.S. de Lemos, Heat transfer in suddenly expanded flow in a channel with porous inserts, in: Proc. of IMECE200—ASME—Int. Mech. Eng. Congr., ASME-HTD-366-5, ISBN 0-7918-1908-6, Orlando, FL, 2000, pp. 191–195.

[30] M. Assato, M.H.J. Pedras, M.J.S. de Lemos, Numerical solution of turbulent channel flow past a backward-facing step with a porous

insert using linear and nonlinear k–ε models, J. Porous Media 8 (1) (2005) 13–29.

[31] R.A. Silva, M.J.S. de Lemos, Numerical analysis of the stress jump interface condition for laminar flow over a porous layer, Numer. Heat Transfer A—Appl. 43 (6) (2003) 603–617.

[32] R.A. Silva, M.J.S. de Lemos, Turbulent flow in a channel occupied by a porous layer considering the stress jump at the interface, Int. J. Heat Mass Transfer 46 (26) (2003) 5113–5121.

[33] R.A. Silva, M.J.S. de Lemos, Laminar flow around a sinusoidal interface between a porous medium and a clear fluid, in: Proc. COBEM2003—17th. Int. Congr. of Mech. Eng., Paper 1528 (on CD-ROM), São Paulo, Brazil, 10–14 November 2003.

[34] M.J.S. de Lemos, R.A. Silva, Turbulent flow around a wavy interface between a porous medium and a clear domain, in: Proc. ASME-FEDSM2003—Fluids Engineering Division Summer Meeting, Paper FEDSM2003-45457 (on CD-ROM), Honolulu, Hawaii, USA, 6–11 July 2003.

[35] A.V. Kuznetsov, L. Cheng, M. Xiong, Effects of thermal dispersion and turbulence in forced convection in a composite parallel-plate channel: investigation of constant wall heat flux and constant wall temperature cases, Numer. Heat Transfer A 42 (2002) 365.

[36] A.V. Kuznetsov, M. Xiong, Development of an engineering approach to computations of turbulent flows in composite porous/fluid domains, Int. J. Thermal Sci. 42 (2003) 913.

[37] A.V. Kuznetsov, S.M. Becker, Effect of the interface roughness on turbulent convective heat transfer in a composite porous/fluid duct, Int. Commun. Heat Mass Transfer 31 (1) (2004) 11.

[38] A.V. Kuznetsov, Numerical modeling of turbulent flow in a composite porous/fluid duct utilizing a two-layer k–ε model to account for interface roughness, Int. J. Thermal Sci. 43 (11) (2004) 1047–1056.

[39] P. Prinos, D. Sofialidis, E. Keramaris, Turbulent flow over and within a porous bed, J. Hydraul. Eng. 129 (9) (2003) 720–733.

[40] W.P. Breugem, B.J. Boersma, R.E. Uittenbogaard, Direct numerical simulations of plane channel flow over a 3D cartesian grid of cubes, in: Proc. of ICAPM2004—International Conference on Applications of Porous Media 2004, Évora, Portugal, 24–27 May 2004, pp. 27–35.

[41] W.P. Breugem, B.J. Boersma, Direct numerical simulations of turbulent flow over a permeable wall using a direct and a continuum approach, Phys. Fluids 17 (2) (2005).

[42] M.J.S. de Lemos, Turbulent kinetic energy distribution across the interface region between a porous medium and a clear fluid, in: Proc. ICTEA—Int. Conf. Thermal Eng. Theory and Applications, Paper ICTEA-TF2-01, Beirut, Lebanon, 31 May–4 June 2004.

[43] M.J.S. de Lemos, Turbulent kinetic energy distribution across the interface between a porous medium and a clear region, Int. Commun. Heat Mass Transfer 32 (1–2) (2005) 107–115.

[44] K. Lee, J.R. Howell, Forced convective and radiative transfer within a highly porous layer exposed to a turbulent external flow field, in: Proc. 1987 ASME–JSME Thermal Engineering Joint Conf., vol. 2, 1987, pp. 377–386.